Proceedings World Geothermal Congress 2020+1
Reykjavik, Iceland, April - October 2021

Introduction of Microseismic Monitoring during Water Injection Test in The Okuaizu Geothermal Field, Japan

Kyosuke Okamoto[1], Yuki Tanaka[1], Hiroshi Asanuma[1], Takashi Okabe[2], Yasuyuki Abe[3] and Masatoshi Tsuzuki[4]

[1]AIST-FREA, 2-2-9, Machiikedai, Koriyama, Fukushima 963-0298, Japan

[2]Geothermal Energy Research & Development Co., Ltd., 22-4, Shinkawa 1-Chome, Chuo-ku, Tokyo 104-0033, Japan

[3]Okuaizu Geothermal Co., Ltd, 1034-1 Sunakohara Kaminodaira, Yanaizu, Fukushima 969-7321, Japan

[4]Japan Oil, Gas and Metals National Corporation, Toranomon Twin Building 2-10-1 Toranomon, Minato-ku, Tokyo 105-0001, Japan

okamoto.kyosuke@aist.go.jp

Keywords: Microseismic monitoring, Seismology, Water injection, Okuaizu

ABSTRACT

A series of water injection tests was conducted for several months in 2015 and 2018 to prevent a reduction in steam production in the Okuaizu Geothermal Field. It is important to understand the spatiotemporal behavior of the injected water in order to control the reservoir system and retrieve steam effectively. For this purpose, microseismic monitoring has been conducted since 2015 using seismic stations deployed to surround the injection well (five stations on the ground surface and four sensors in the borehole). In this paper, we outline the hardware and software systems of a microseismic monitoring network and the procedure for estimating water flows using the microseismic data. As a result, we found that high-resolution hypocenter determinations, using a cluster analysis, can illuminate the subsurface water flow path precisely.

1. INTRODUCTION

During injection of water into geothermal reservoirs, it is important to monitor and control the migration of fluid to avoid cooling of the reservoir and to retrieve steam efficiently. For this purpose, microseismic monitoring has been widely used to determine the spatiotemporal behavior of reservoirs (e.g., Fehler et al., 1987; Baria et al., 1999). In the Okuaizu Geothermal Field (OGF), Japan, water injection tests were conducted in 2015 (Okabe et al., 2016; Kato et al., 2020) and 2018. Between 2015 and 2018, the injection well was repaired, and the feed points were changed. The total amount of injected water in the 2015 tests (approximately 1.7×10^5 m^3) was relatively larger than that in 2018 (approximately 2.9×10^3 m^3). In this paper, we introduce an overview of the seismic monitoring system in OGF. Using the seismic data, we conducted a high-resolution hypocenter determination using the double-difference method (DD, Waldhauser and Ellsworth, 2000) to understand the behavior of the injected water (Okamoto et al., 2018). We also report differences between the microseismic events associated with the water injection tests in 2015 and 2018.

As part of the “Technology to Evaluate and Manage Geothermal Reservoirs” project, conducted by the Japan Oil, Gas and Metals National Corporation (JOGMEC) (e.g., Okabe et al., 2016), a continuous water injection (without pressurization) test was conducted in OGF, Fukushima, Japan (Figure 1 (left)) from June to August and November to December in 2015 and from November to December in 2018, in an effort to stop the reduction of steam production. The main differences between the injection tests in 2015 and 2018 are the total volume of injected water and the injection rate. The feed points are also considered to be different between these tests because repair of the injection well was started after the end of the injection test in 2015 and completed in 2019. An undesirable leak of injected water from the injection well, which interfered with an adjacent well, was found during the injection tests in 2015. The water injection test in 2018 was conducted using the injection well that was being repaired; details of the repairs are in Kato et al. (2020). Seismic data were continuously recorded using five seismic stations on the surface and four borehole sensors (the maximum installation depth is around 400 m), which JOGMEC has deployed since 2015; we called this seismic network—YAE. From the YAE records, microseismic events were determined using manually picked P- and S-wave arrivals. Figure 1 (right) shows the geometry of the YAE seismic stations and the injection well (the well trace at the time, in 2015, is shown). Besides the YAE seismic stations, the Okuaizu Geothermal Co., Ltd. (OAG) also deployed five seismic stations (event trigger type) on the surface; we called this seismic network—OMS (this is not used in this study).

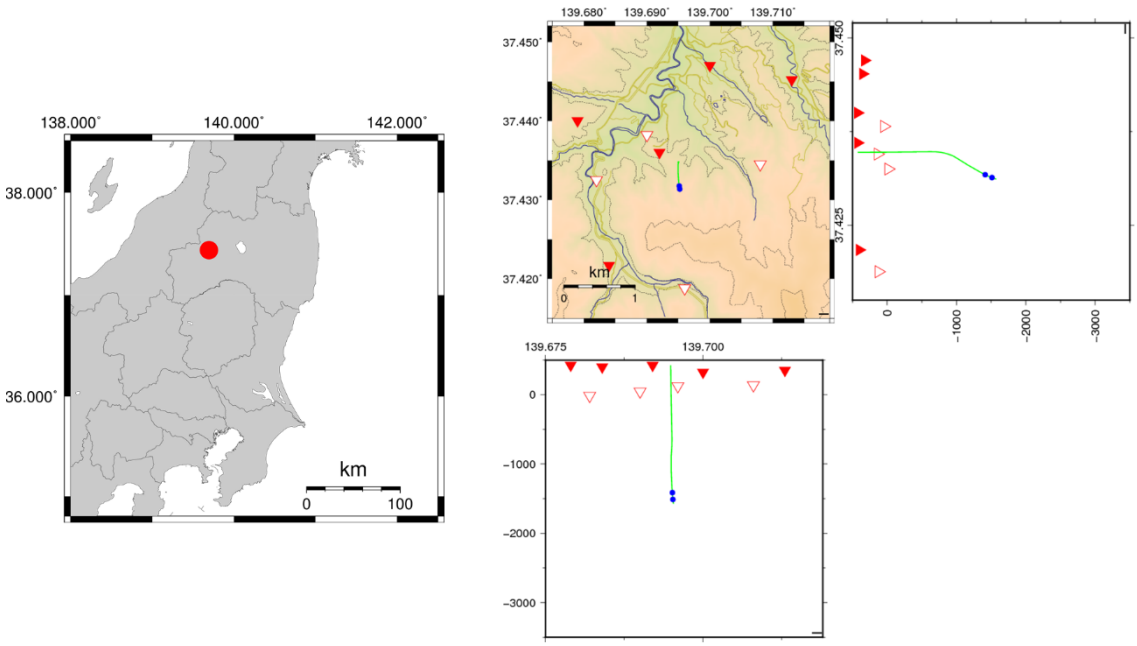

Figure 1: (Left) Location of the Okuaizu Geothermal Field. (Right) Geometry for the injection well (the green line with the injection point shown by the blue circle) and seismic stations (borehole sensor: white triangle; sensor on the surface: red triangle).

2. OUTLINE OF THE INJECTION TESTS

2.1 Injection tests in 2015

The total volume of injected fluid was approximately 1.7×10^5 m^3. The 2015 injection tests were composed of the first injection test (1.2×10^5 m^3) and the second injection test (0.5×10^5 m^3) with approximately three months gap between them. The duration of the first and second injection tests was about 3 months and 1 month, respectively. Both the injection tests were started from an initial step rate test of around 50 to 70 t/m^3. After the initial step rate test, the injection rate was fixed at 50 m^3/h (1.39×10^{-2} m^3/s), and then increased to 70 m^3/h (1.94×10^{-2} m^3/s) in the first injection test. In the second injection test, a rate of 70 m^3/h (1.94×10^{-2} m^3/s) was used after the initial step rate test. The injection target area was a heating zone in the geothermal field.

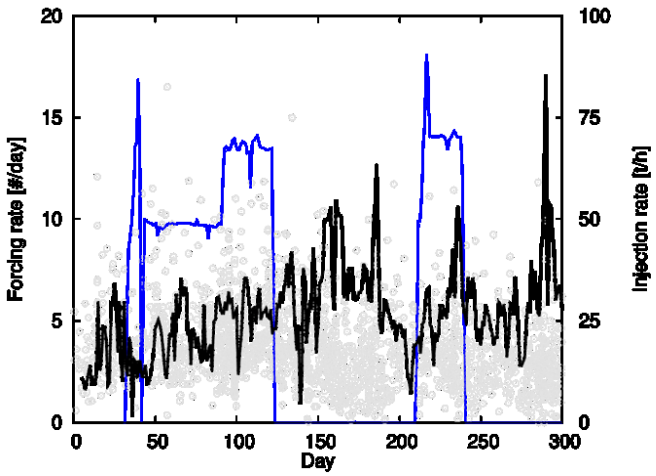

Figure 2: Time history of injection rate (blue line) and forcing rate (black line) for the 2015 injection tests. The day count started on May 1, 2015.

We conducted a statistical analysis using the epidemic-type aftershock sequence (ETAS) model (Ogata, 1988), which is an appropriate tool for extracting the primary fluid signal from background natural seismicity (Hainzl and Ogata, 2005). In the ETAS model, it is assumed that each seismic event can produce aftershocks which follow the Omori law of the main seismic event. The whole seismicity is described by the superposition of aftershocks for all the events, as well as seismic events which do not follow the Omori law. The latter seismic events are considered to be derived from non-natural activities (i.e., here, water injection). The number of the non-natural seismic events a day (known as forcing rate, (#/day)) is described by the black line in Figure 2. The forcing rate

increased within several tens of days after the start of the first injection test. It continued to increase after the termination of the first injection test and decreased to the original state of the pre-injection term around the day 200. Associated with the start of the second injection test, the forcing rate sharply increased again.

2.2 Injection test in 2018

The total volume of injected fluid was approximately 2.9×10^3 m^3. The initial stage of the injection test was started with step rate test of approximately 10 m^3/h (2.78×10^{-3} m^3/s), and subsequently the injection rate was fixed to approximately 5 m^3/h (1.39×10^{-3} m^3/s). The duration of the injection was approximately 1 month. The values of the total injected volume, injection rate, and duration time are less than those of the 2015 injection tests. The injection rate and forcing rate are shown in Figure 3. The forcing rate appears not to correlate with the injection rate. It does not show the characteristic behavior associated with the start of the injection, unlike the 2015 injection tests.

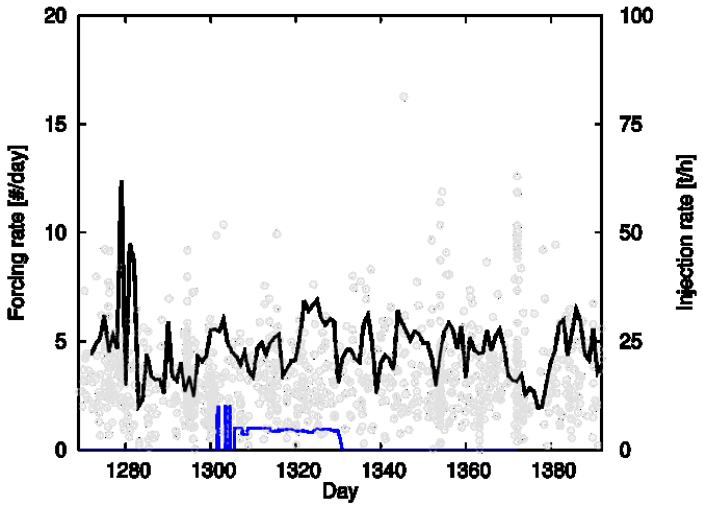

Figure 3: Time history of injection rate (blue line) and forcing rate (black line) for the 2018 injection test. The day count started on May 1, 2015.

3. MICROSEISMIC MONITORING SYSTEM

Continuous seismic records were observed at the YAE seismic stations shown in Figure 4. Each seismic station was equipped with batteries and solar panels, or connected to a commercial power supply. Therefore, they could record continuous seismic records every day. The surface sensors were Trillium Compact Posthole 20s (Nanometrics Inc.); they were manually buried under the ground surface. The borehole sensors were F41-15.0 (International Earth Sciences IESE Ltd.), installed at depths of approximately several hundred meters. The logger we employed was the Centaur digital recorder (Nanometrics Inc., Figure 4 (right)). The sampling rate was 1,000 Hz.

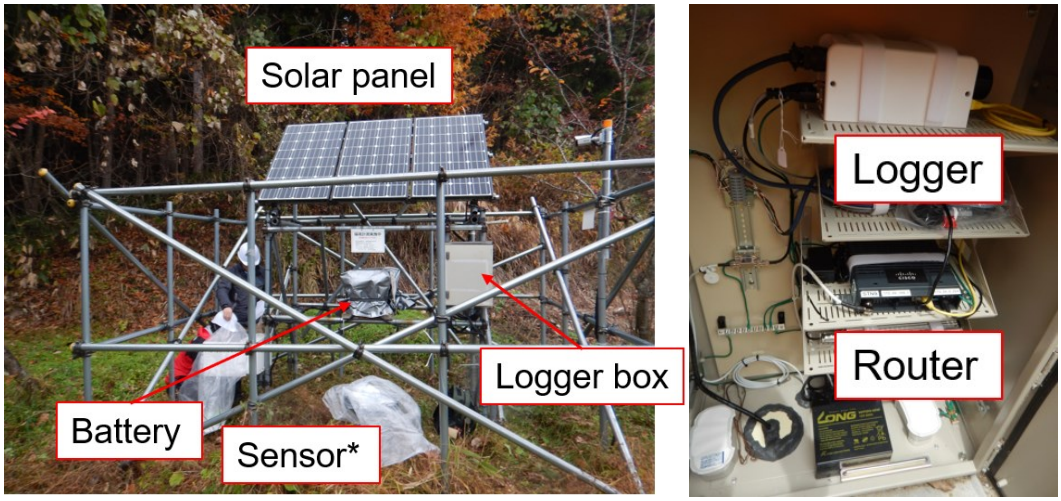

Figure 4: (Left) Overall view of a seismic station. (Right) View inside the logger box.

The record observed at each seismic station was transferred to a remote local server in OAG via a 3G wireless network and integrated in real time by the Apollo server. Then, the integrated data were transferred to a server at the National Institute of Advanced Industrial

Science and Technology (AIST) (Figure 5). We checked the data every day and picked P- and S-wave arrivals for daily hypocenter determination, which was calculated using the Geiger's method.

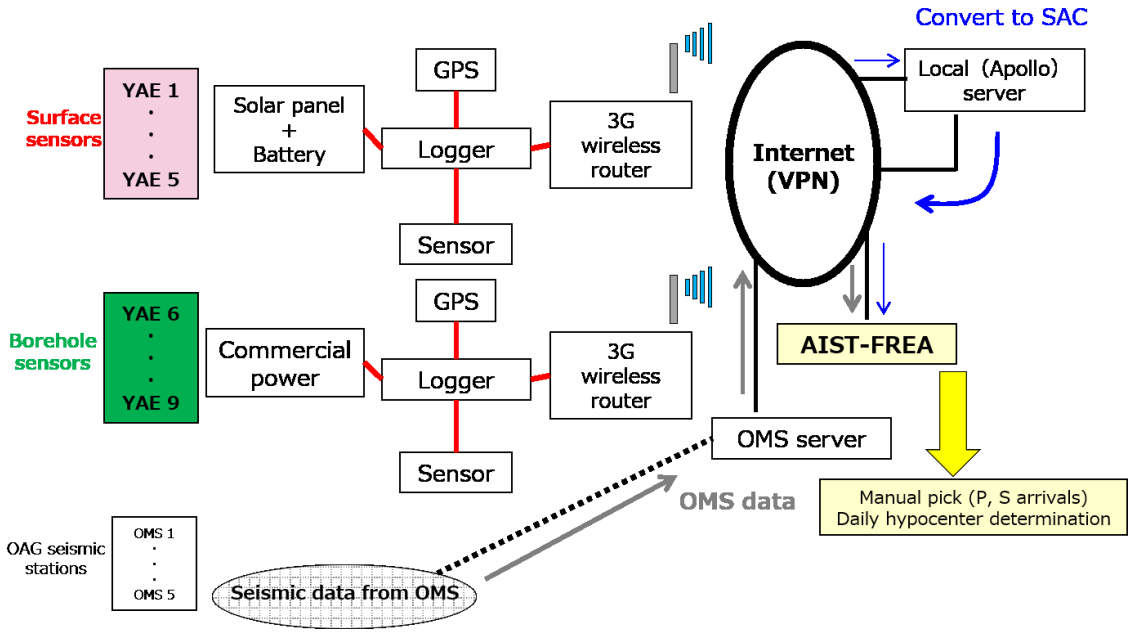

Figure 5: Overview of microseismic monitoring system.

We employed a cluster analysis of microseismic events to determine more precise locations of the events associated with the injection tests. The analysis was applied to the daily-determined seismic events. Clusters of microseismic events were identified by cross-correlation of the waveforms (e.g., Schaff et al., 2004) of the up-down (UD) component in the 20–80 Hz frequency range of sensors. The relative difference times in the P-wave arrivals for seismic pairs in a cluster were calculated on the basis of the cross-correlation to create the input for the DD method. The spatial residuals were in the order of 10 m after the hypocenters were relocated; the centroid of a cluster was used for routine hypocenter determination.

4. MICROSEISMIC DISTRIBUTIONS ASSOCIATED WITH THE INJECTION TESTS

4.1 Injection tests in 2015

We divided the analysis term into five sub-parts as follows: (a) pre-injection term before the start of the first injection test (1 month), (b) during the first injection test (3 months), (c) interval between the first and second injection tests (3 months), (d) during the second injection test (1 month) and (e) post-injection term after the termination of the second injection test (1 month). The corresponding results of the microseismic events are shown in Figures 6a–e.

Before the injection tests, active seismicity was seen in an area northeast of the injection well (Figure 6a). The location is approximately on an existing fault (New Energy Development Organization, 1997). Areas around the injection well were not seismically active at that time. As the first injection test started, active microseismic clusters were created in the areas around the injection well (Mqs1) as well as at the existing fault (Mqs2) (Figure 6b). There was an aseismic zone between the areas of Mqs1 and Mqs2. After the termination of the first injection test, a new microseismic cluster (Mqs3) was created near the injection well (Figure 6c). Although both Mqs1 and Mqs3 were created near the bottom of the injection well (within several hundred meters), their locations were slightly different to each other. The microseismic clusters above (Mqs1, Mqs2 and Mqs3) were all likely derived from the injection operation, according to the rise of the forcing rate in the ETAS analysis (see Figure 2). The activity of Mqs3 had calmed down before the second injection test started. The activity at Mqs1 and Mqs2 was excited again, probably associated with the second injection test (Figure 6d), because the forcing rate also started to rise again (Figure 2). The precise locations of Mqs1 and Mqs2 in the second injection test moved slightly from those in the first injection test. In the second injection test, their locations seemed to shift towards the periphery of the original locations of Mqs1 and Mqs2 in the first injection test. On the other hand, Mqs3 was not activated after the termination of the second injection test, unlike with the first injection test.

4.2 Injection test in 2018

We divided the analysis term into 3 sub-parts as follows: (a) pre-injection term before the start of the injection test (1 month), (b) during the injection test (1 month) and (c) post-injection term after the termination of the injection test (1 month). The corresponding results of microseismic events are shown in Figures 7a–c.

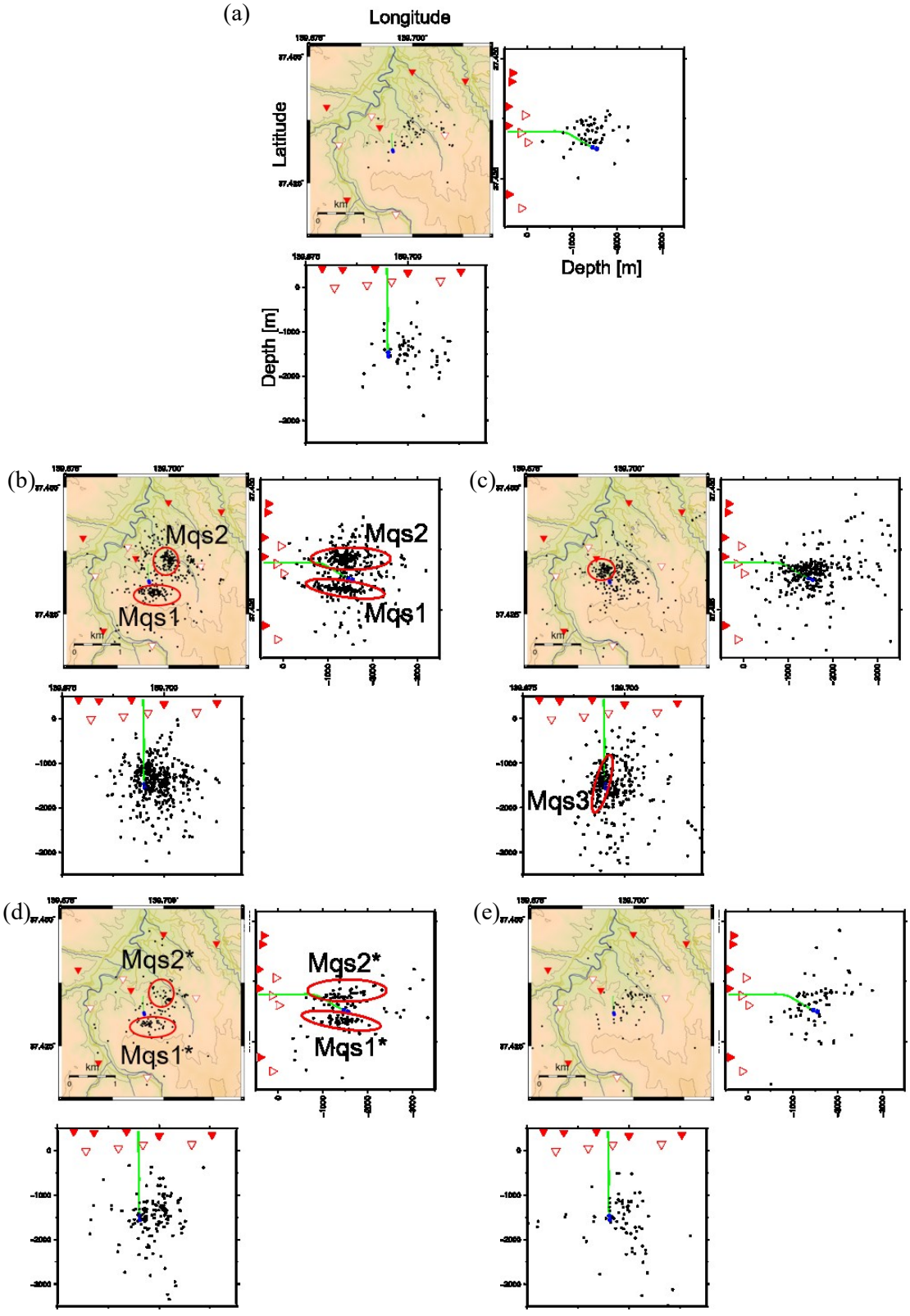

Figure 6: Hypocenter distributions (map view and N-S and E-W cross-sections) for the 2015 injection tests. (a) pre-injection term before the start of the first injection test (1 month), (b) during the first injection test (3 months), (c) interval between the first and second injection tests (3 months), (d) during the second injection test (1 month) and (e) post-injection term after the termination of the second injection test (1 month).

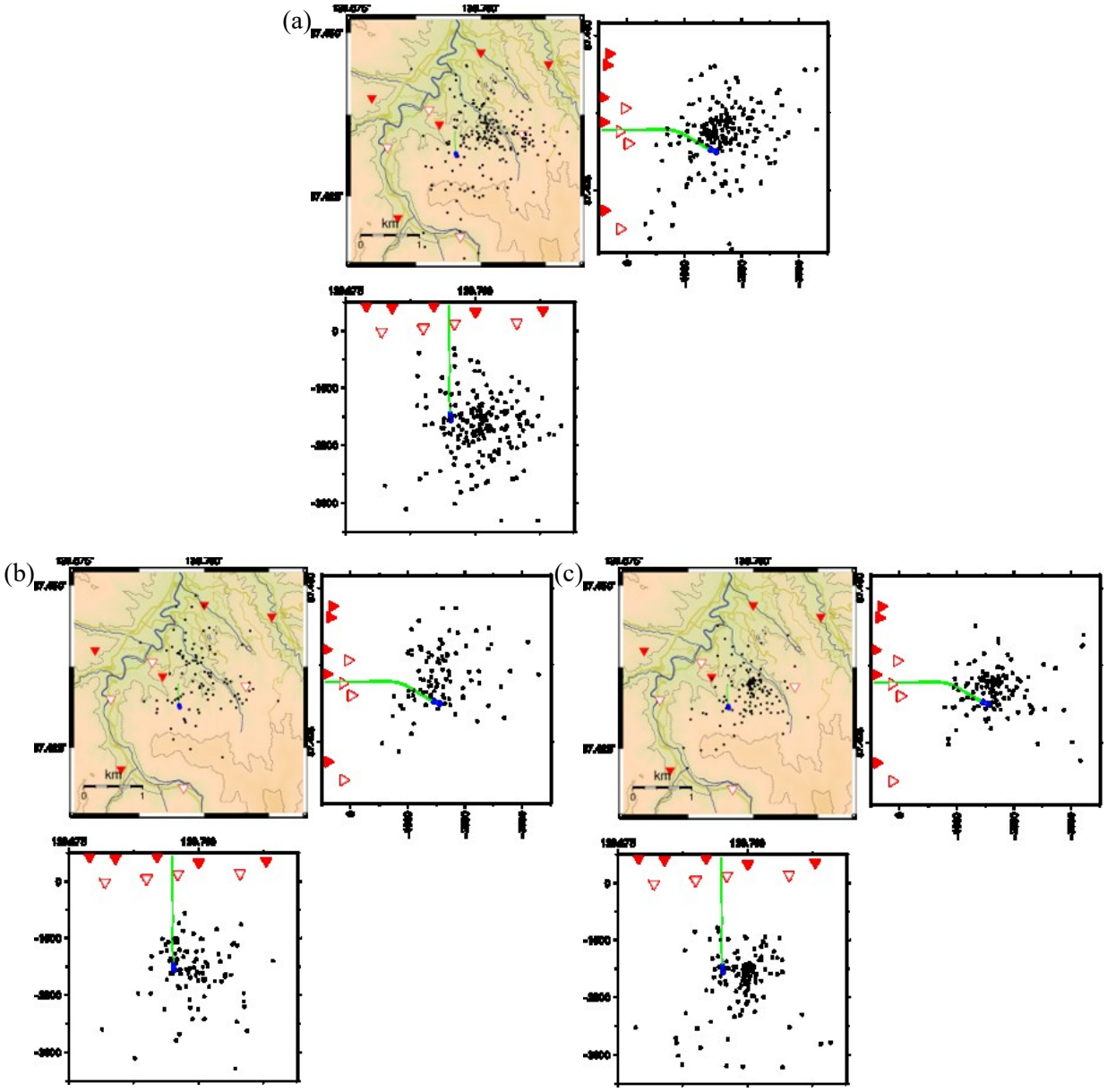

Figure 7: Hypocenter distributions (map view and N-S and E-W cross-sections) for the injection 2018 test. (a) pre-injection term before the start of the injection test (1 month), (b) during the injection test (1 month) and (c) post-injection term after the termination of the injection test (1 month).

Seismicity before the injection test (Figure 7a) was more active than the corresponding pre-injection term in 2015 (Figure 6a). The seismically active area seemed to be on the existing fault, and areas around the injection well were seismically inactive in a similar manner to the 2015 injection tests. During the injection test, seismicity on the existing fault became lower and the microseismic clusters around the injection well (e.g., Mqs1 and Mqs3 in the 2015 injection test) were not activated (but there were a few microseismic events near the feed points of the injection well, Figure 6b). The forcing rate in the ETAS analysis did not show a characteristic change during the injection test (see Figure 2). The microseismicity on the existing fault was activated again after the termination of the injection test (Figure 7c).

5. DISCUSSION

Microseismic events associated with water injection were clearly created in the 2015 injection tests, while they were not obvious in the 2018 injection test. Rather, the seismicity seemed to calm down during the 2018 injection test. The main differences between the injection tests in 2015 and 2018 are the total volume of injected water and the injection rate. These factors could lead to the different seismic characters in 2015 and 2018. Another possible factor is the repair of the injection well after the injection tests in 2015 (see Kato et al., 2020). The depths of feed points might differ between the injection tests in 2015 and 2018. It is uncertain whether the lower activity of microseismicity during the injection, compared to the post- and pre-injection terms in 2018, was derived from the injection operation.

Figures 7a and b show cross-sections of Mqs1, Mqs2, and Mqs3 projected on a migration image produce from S-coda waves of seismic events in 2015 and 2016 (Okamoto et al., 2018). It is assumed that the migration image indicates the location of fractures. According to the images, Mqs1 and Mqs2 were located at the periphery of a fracture; the injected water might flow through the fracture without seismicity. Mqs3 was located on another fracture near Mqs1 and Mqs2. The location of Mqs3 might be a newly created permeable zone after the shut-in.

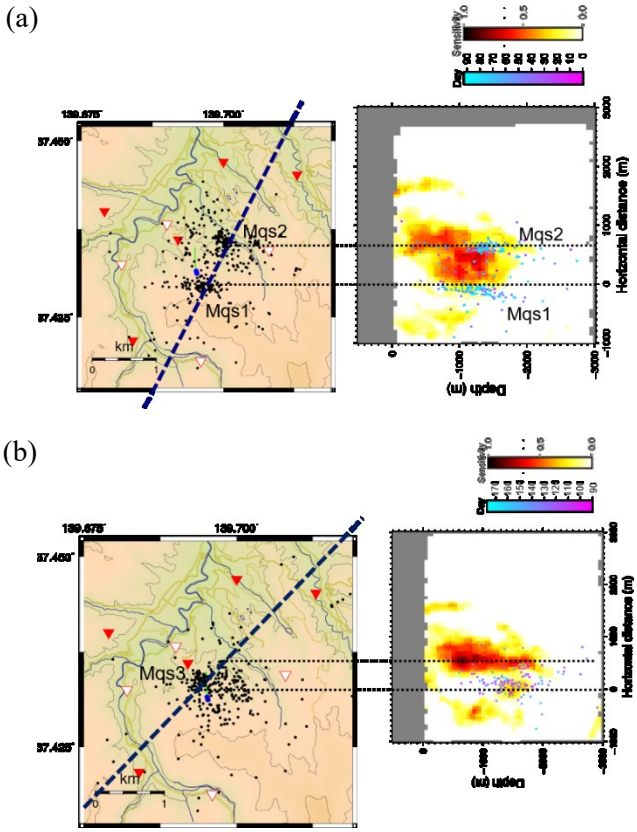

Figure 7: Cross-section of microseismic clusters and the migration image produced by S-coda waves. The blue dashed line is the transverse line of the cross-section in map view. The term is (a) during the first injection test in 2015 and (b) after the termination of the first injection test.

6. SUMMARY

In this paper, we introduced an overview of a microseismic monitoring system (software as well as hardware) in OGF. Microseismic events associated with the injection tests in 2015 and 2018 were analyzed using the microseismic monitoring system. We evaluated the results of hypocenter determination and found different features between the 2015 and 2018 tests. Microseismic clusters were excited during the injection and the post-injection terms in 2015, while a few microseismic events occurred during the injection test in 2018. The contradictory features in microseismicity may be derived from the differences in injection volume, injection rate, and feed points between 2015 and 2018.

The injection test for deeper depths, using the repaired injection well, began on July 2 2019 after PTS logging and the setting of the pressure and temperature monitoring tool. We are continuing to monitor the microseismicity and evaluate the microseismic events associated with the injection tests (note that this paper was written in July 2019).

REFERENCES

Baria, R., Baumgärtner, J., Gérard, A., Jung, R., and Garnish, J.: European HDR research program at Soultz-sous-Forêts (France) 1987-1996, *Geothermics*, **28**, (1999), 655–669.

Fehler, M., House, L., and Kaieda, H.: Determining planes along which earthquakes occur: Method and application to earthquakes accompanying hydraulic fracturing, *J Geophys Res*, **92**, (1987), 9470–9414.

Hainzl, S., and Ogata, Y.: Detecting fluid signals in seismicity data through statistical earthquake modeling, *J. Geophys. Res.*, **110**, (2005), doi: 10.1029/2004JB003247.

Kato, M., Okabe, T., Sato, T., Nakata, H., Abe, Y., Asanuma, H., Okamoto, K., Yoshimatsu, K., Kamenosono, H., and Tsuzuki, M.: Progress of the EGS project for water injection in the superheated region at Okuaizu geothermal field in Japan, *Proceedings*, World Geothermal Congress 2020, Raykjavik, Iceland (2020).

New Energy Development Organization: Geothermal development promotion survey No. B-1 “Sarukuradake Area”: Geothermal development research report. Available via http://geothermal.jogmec.go.jp/gathering/file/42.pdf, (1997), Accessed 29 Nov 2017

Ogata, Y.: Statistical models of point occurrences and residual analysis for point processes, *J. Am. Stat. Assoc.*, **83**, (1988), 9-27.

Okabe, T., Kato, M., Sato, T., Abe, Y., Asanuma, H., Oishi, T., and Tosha, T.: Current status of the EGS project for water injection in the superheated region at Okuaizu Geothermal Field in Japan, *Proceedings*, 38th New Zealand Geothermal Workshop, Auckland, New Zealand (2006).

Okamoto, K., Yi, L., Asanuma, H., Okabe, T., Abe, Y., and Tsuzuki, M.: Triggering processes of microseismic events associated with water injection in Okuaizu Geothermal Field, Japan, *Earth, Planets and Space*, **70**, (2018), doi: 10.1186/s40623-018-0787-7.

Schaff, D.P., Bokelmann, G.H.R., Ellsworth, W.L., Zanzerkia, E., Waldhauser, F., and Beroza, G.C.: Optimizing correlation techniques for improved earthquake location, *Bull Seism Soc Am*, **94**, (2004), 705–721.

Waldhauser, F., Ellsworth, W.L.: A double-difference earthquake location algorithm: Method and application to the Northern Hayward Fault, California, *Bull Seism Soc Am*, **90**, (2000), 1353–1368.